Thermally-activated creep and fluidization in flowing disordered materials

SAMY MERABIA, FRANÇOIS DETCHEVERRY

Univ Lyon, Université Claude Bernard Lyon 1, CNRS, Institut Lumière Matière, F-69622, VILLEURBANNE, France

Abstract –When submitted to a constant mechanical load, many materials display power law creep followed by fluidization. A fundamental understanding of these processes is still far from being achieved. Here, we characterize creep and fluidization on the basis of a mesoscopic viscoplastic model that includes thermally activated yielding events and a broad distribution of energy barriers, which may be lowered under the effect of a local deformation. We relate the creep exponent observed before fluidization to the width of barrier distribution and to the specific form of stress redistribution following yielding events. We show that Andrade creep is accompanied by local strain hardening driven by stress redistribution and find that the fluidization time depends exponentially on the applied stress. The simulation results are interpreted in the light of a mean-field analysis, and should help in rationalizing the creep phenomenology in disordered materials.

Introduction. – Creep is observed in a variety of systems including crystalline metals [1], soft crystals [2], polymeric, metallic and colloidal glasses [3–7], gels [8,9], and everyday complex fluids [10]. Typically, the strain first increases with time following a power law regime often described as Andrade creep, with $\epsilon(t) \sim t^p$ and an exponent p between 0 and 1. This creep regime is eventually interrupted by fluidization, after an elapsed time that decreases with the applied stress. Though the creep phenomenology is widespread, to date its understanding remains only partial [11,12], in particular for the underlying physical mechanism at play. Creep in metals is traditionally interpreted in terms of depinning and collective motion of dislocations [1,13]. No such framework exists for disordered materials.

While molecular simulations may provide a wealth of information on mechanical properties [6,14], the slow kinetics inherent to creep make it prohibitive to reach fluidization time. Following the pioneering work of Bulatov and Argon [15], mesoscopic models appear as an alternative to bridge both time and length scales between the molecular level and macroscopic, finite elements calculations [14]. The common idea is to coarse-grain fast microscopic motions, and retain only a minimal description of local plastic rearrangements or shear transformation zones (STZs), most importantly the long-range consequences of a single localized plastic event. Therefore, the essential ingredients include a local yielding probability, and a spatially resolved dynamics for the stress redistribution, often described by an Eshelby form. Whereas elasto-plastic models have now generated a sustained line of research [12,16–18], with much scrutiny on the shear steady state, comparatively little attention has been devoted to analyze the creep dynamics. Two noticeable exceptions are a spatially resolved Soft Glassy Rheology model [19] and a recent study by Bouttes and Vandembroucq [20], which, however, is restricted to logarithmic creep only.

The purpose of this letter is to propose an interpretation of creep on the basis of a mesoscopic model. We focus on the situation where i) thermally-activated yielding events play the leading role, ii) disorder induces a wide distribution of activation barriers, iii) there is no yield-stress. Using numerical simulations and a mean-field analysis, we investigate how the creep exponent is related to the barrier distribution and examine the influence of the stress redistribution on the creep dynamics. Interestingly, our model reveals local strain hardening during the creep regime: local stress may accumulate in some regions, while in others, it decreases with the global shear rate. Such strain hardening phenomenon, which differs from that seen in metals, eventually triggers the fluidization and allows to propose a simple law for the fluidization time.

Model. – Our mesoscopic description relies on three main ingredients: a distribution of yielding barriers, possibly modified by mechanical effect, thermal activation, and stress redistribution. The system is divided into a collection of representative elements whose dimension corresponds to the size of a plastic event, and whose state is specified by an intrinsic energy barrier E and a local mechanical stress σ, assumed to be a scalar for simplicity. In a way similar to Eyring's model, thermal activation can trigger yielding with a rate

$$\lambda(E, \sigma) = \tau_{\mathrm{m}}^{-1} \exp\left[-\frac{E - h(\sigma)}{k_B T}\right]. \tag{1}$$

Here, τ_{m} is a microscopic time, k_B is the Boltzmann constant and T is the temperature. The function $h(\sigma)$ specifies how the barrier may be lowered by the local stress; we will mainly consider a quadratic mechanical activation term $h(\sigma) = \sigma^2 v_a/(4\mu k_B T)$, where v_a is an activation volume, μ the infinite frequency shear modulus [21]. After yielding, an element has his intrinsic barrier renewed from a distribution $\rho_{\mathrm{E}}(E)$, its local stress put to zero, and the stress it carried is redistributed to other elements.

Three types of stress redistribution are possible: "Eshelby", "mean-field" and "short-range". The first propagator, which originates in the Eshelby problem of an inclusion in an elastic matrix, is quadrupolar [16, 22]

$$G_{ij} = \frac{2}{\pi r_{ij}^2} \cos(4\theta_{ij}) \tag{2}$$

where G_{ij} is the contribution received by site i from a site j, $r_{ij} = |\mathbf{r}_{ij}|$ is the distance between the two sites, and $\cos\theta_{ij} = (\mathbf{r}_{ij} \cdot \mathbf{e}_x)/r_{ij}$, with $\mathbf{e}_x$ a unit vector along the direction of shear. The mean-field propagator completely neglects spatial dependence and assign to all elements an identical contribution $G_{ij} = 1/(N-1)$, N being the total number of sites. To further assess the influence of the redistribution type, we will also consider a short-range propagator [23], for which the stress carried by an element is redistributed only to its nearest neighbours, as described in Ref. [24]. Note that only the Eshelby propagator is physically sound, the others are considered for comparison purpose.

To fully specify the model, it remains to choose the probability density of intrinsic barrier energy $\rho_{\mathrm{E}}(E)$. In the following, we will concentrate mostly on a Gaussian distribution with mean $\bar{E}$ and variance Δ^2,

$$\rho_{\mathrm{E}}(E) = \frac{1}{\sqrt{2\pi\Delta^2}} \exp\left[-\frac{(E - \bar{E})^2}{2\Delta^2}\right]. \tag{3}$$

Such a Gaussian form is often assumed in modelling the plastic behaviour of polymer glasses [25], or more generally molecular glasses [26, 27]. Furthermore, it has long been recognized to be associated with a stretched exponential relaxation functions [27, 28]. For the sake of analytical tractability, we will also consider a barrier distribution
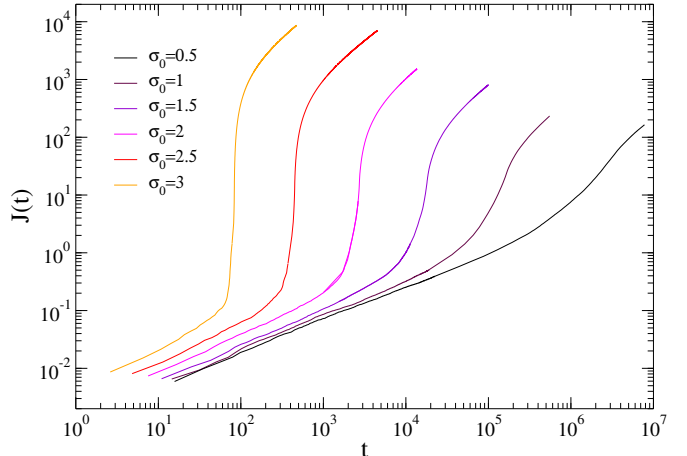

Fig. 1: Creep compliance in simulations. The stress redistribution is of Eshelby type, and the distribution of energy barrier is Gaussian with $\Delta = 3$. Different values of applied stress σ_{o} are shown.

which is exponential and has a width α^{-1},

$$\rho_{\mathrm{E}}(E) = \alpha \exp\left[-\alpha(E - E_o)\right] H[E - E_o], \tag{4}$$

where E_o denotes the minimal energy barrier and H is the Heaviside distribution. The model is close to that of Ref. [20], but the distribution of energy barriers has a width which is finite rather than infinite, hence logarithmic creep is never observed.

Simulations. – To solve the model numerically, we discretize space with a two-dimensional square lattice and periodic boundary conditions. Initially, each site i carries the same stress σ_0, and is assigned an energy barrier E_i sampled from the steady distribution $\rho_E(E_i)\exp(E_i/k_B T)$. The creep process is simulated using a Kinetic Monte Carlo (KMC) algorithm [29]. Given the yielding rates specified by Eq. (1) for all sites, each iteration selects a site i to yield, and generates a corresponding time increment. Upon yielding, the local stresses and the total strain are updated as follows,

$$\sigma_i \to 0, \quad \sigma_j \to \sigma_j + G_{ij}\sigma_i^- \text{ for } j \neq i, \quad \epsilon \to \epsilon + \sigma_i^-/2\mu, \tag{5}$$

where σ_i^- is the stress carried by the site i prior to yielding. A new energy barrier is then chosen from the probability density ρ_E. We use a pseudo-spectral method to carry out the elastic redistribution [16], and impose the sum rule $\forall i, \sum_{j \neq i} G_{ij} = 1$, so that the spatially averaged stress $\frac{1}{N}\sum_i \sigma_i = \sigma_0$ remains constant at all time, as required by the creep set-up. We have simulated systems with typical linear size 64 and 256, and verified that the results are not size dependent. In data presented below, we take $k_B T$ as energy unit, express stress in units where the shear modulus is $\mu = 1$, and choose the time unit as $\tau_{\mathrm{m}}\exp(\bar{E})$ or $\tau_{\mathrm{m}}\exp(E_o)$ in the Gaussian and exponential case respectively. Finally, the activation parameter is

set to $v_a = 1$. Once this choice is made, the only remaining parameter of the model is the distribution width Δ or α^{-1}. If not indicated otherwise, the stress redistribution is of Eshelby form, and $\rho_{\rm E}$ is Gaussian.

Figure 1 summarizes the creep phenomenology of our model. Whatever the applied stresses $\sigma_{\rm o}$, three regimes may be distinguished in the compliance curve $J(t) = \epsilon(t)/\sigma_{\rm o}$. At early times, the compliance increases algebraically with time $J(t) \sim t^p$, where the creep exponent p is found to be almost independent of $\sigma_{\rm o}$. This first regime terminates with a sharp increase in deformation, at a fluidization time $t_{\rm f}$ that decreases with the applied stress $\sigma_{\rm o}$. The system eventually settles into steady flow, where the strain increases linearly with time, $J(t) \sim t$. Below we investigate in turn the primary creep and fluidization. To do so, we now develop a mean-field theory.

Mean-field analysis. – When spatial dependence is entirely discarded, the system is completely described by the probability density $P(E, \sigma, t)$ to find at time t an element with energy barrier E and subject to a stress σ. Our starting point is the evolution equation

$$\partial_t P = -\lambda(E,\sigma)P + Y(t)\rho_{\rm E}(E)\delta(\sigma) - S(t)\partial_\sigma P, \quad (6)$$

where $Y(t) = \langle\lambda(E,\sigma)\rangle_P$, $S(t) = \langle\sigma\lambda(E,\sigma)\rangle_P$ and $\langle.\rangle_P$ denotes an average over the full distribution $P(E,\sigma,t)$. In the RHS of Eq. (6), the first term originates from elements in state (E,σ) that yield with a rate $\lambda(E,\sigma)$. $Y(t)$ is the average yielding rate, also called material's fluidity [19]. Elements that have yielded arrive in a renewed state with zero stress and an energy barrier randomly chosen in the distribution $\rho_{\rm E}(E)$. The average rate of released stress $S(t)$ gathers the contributions from all yielding elements, which is redistributed equally throughout the system, resulting in a drift term in σ with velocity $S(t)$. One can check that the evolution equation implies two conserved quantities: the total probability and the total stress. While Eq. (6) may be written directly, a derivation is possible starting from a Boltzmann equation involving a stress collision operator.

The model defined here is related to but distinct from the Soft Glassy Rheology (SGR) model [30]. With quadratic activation function $h(\sigma) \sim \sigma^2$ and an exponential $\rho_{\rm E}(E)$, the model is formally equivalent to SGR with noise temperature $x = \alpha$. However, the interpretation is completely different, since as in the original trap model [28], T here is really the temperature, not an effective noise resulting from yielding events elsewhere in the material. It was pointed out that the mechanical noise in SGR should be "determined self-consistently by the interactions in the system" [31]. This key point is captured by the redistribution term $S(t)\partial_\sigma$, and is crucial for the creep situation, a transient regime. In contrast to steady shear where the noise temperature is constant, the activity here is time-dependent, as it slowly declines during creep. Our description is also reminiscent of fiber bundles model (FBM) but differs in an essential way [32,33]. In contrast

to fibers that permanently disappear once ruptured, elements that have yielded are renewed and will again carry a stress. The mean-field analysis is used in the following to provide a qualitative understanding ; to a large extent, it proves sufficient to rationalize what occurs in more realistic cases.

Creep regime. – We first consider the mean-field model and seek the total strain $\epsilon(t) = \int_0^t S(t)/2\mu$ that follows a stress step. The model can be solved if we neglect non-linear effects by setting $h(\sigma) = 0$. In that case, the yielding of an element depends only on the time elapsed since its latest renewal and $Y(t)$ can be computed without any reference to the local stress. The distribution of barriers is in a steady state characterized by

$$P_{\rm st}(\tau) = \frac{\tau\rho(\tau)}{\langle\tau\rangle}, \qquad Y_{\rm st} = \frac{1}{\langle\tau\rangle}, \quad (7)$$

where, from now on, we use the intrinsic yielding time $\tau = e^E$ rather than the energy barrier, and $\langle.\rangle$ denotes an average over the corresponding distribution $\rho(\tau)$. The initial condition involves a uniform load on all elements and an equilibrated distribution of barriers, namely $P(\tau,\sigma,t=0) = P_{\rm st}(\tau)\delta(\sigma - \sigma_{\rm o})$. We do not consider aging effects.

To solve the model, let us introduce $\overline{\sigma}(\tau,t) = \int d\sigma\sigma P(\tau,\sigma,t)$ which satisfies

$$\partial_t\overline{\sigma} = -\frac{\overline{\sigma}}{\tau} + S(t)P_{\rm st}(\tau), \quad S(t) = \int\frac{d\tau}{\tau}\overline{\sigma}(\tau,t). \quad (8)$$

Using the condition $\int d\tau\,\overline{\sigma}(\tau,t) = \sigma_{\rm o}$ that holds at all time, and working with Laplace transforms, one obtains the exact solution, valid for any distribution of barriers,

$$\frac{S(s)}{\sigma_{\rm o}} = \frac{1}{sR(s)} - 1, \quad R(s) = \int d\tau\frac{P_{\rm st}(\tau)}{s + \tau^{-1}}, \quad (9)$$

where s is the Laplace variable and indicates the nature of the function. Note that Eq. (9) can be rewritten as $J(s)G(s) = 1/s^2$, where $J(s) = \epsilon(s)/\sigma_{\rm o}$ is the compliance, and $G(s) = \mu R(s)$ is the relaxation modulus [34]. The explicit expression $G(t) = \mu\int_0^\infty P_{\rm st}(\tau)e^{-t/\tau}d\tau$ has a simple interpretation. The integral is the average fraction of elements that have never yielded at time t, suggesting that sites that have already yielded at least once do not play any role, as if disappearing in FBM-like models. This interpretation is surprising at first sight but understandable with the analysis of local stress presented below.

Though $R(s)$ can be obtained in closed form for some barrier distributions, taking the inverse Laplace transform of $1/R(s)$ proves impossible. Accordingly, we resort to a small-s expansion and relying on Tauberian theorems [35], we extract the asymptotic behavior of $S(t)$. For the sake of tractability, we consider an exponential distribution of barrier as defined in Eq. (4), which translates into a power law distribution of yielding time $\rho(\tau) = \alpha\tau_o^\alpha/\tau^{\alpha+1}H[\tau - \tau_o]$, with τ_o the minimum value. Assuming $\alpha > 1$, $R(s)$ can be expressed in terms of hypergeometric function as
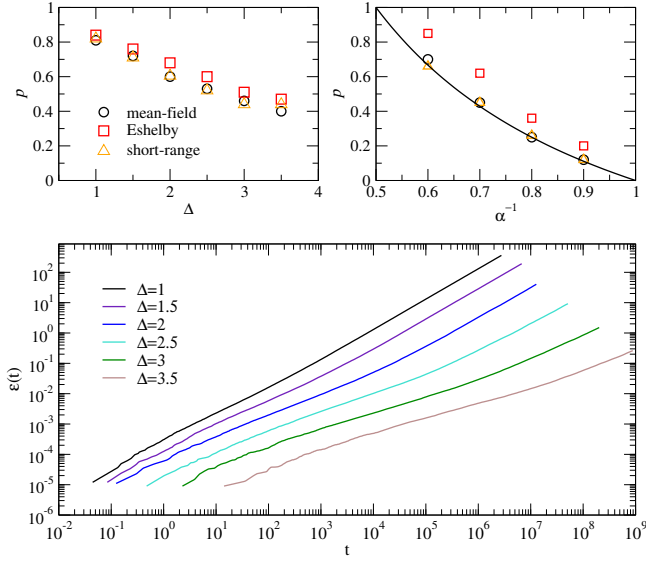
Fig. 2: Creep regime and exponent. (Bottom) Strain curves with Eshelby redistribution and Gaussian ρ_E of various widths Δ. The applied stress is $\sigma_o = 0.01$. (Top) Creep exponent, as defined in the text, for three types of stress propagators, and for Gaussian and exponential ρ_E (left and right respectively). In the latter, the line is the mean-field prediction. Symbol size is indicative of error bars.

$sR(s) = {}_2F_1\left(1, -1+\alpha, \alpha, -1/\tau_o s\right)$. Several cases arise for the asymptotic behavior. If $\alpha > 2$, then the long-time behavior is Newtonian with $S(t) \sim \langle\tau\rangle/\langle\tau^2\rangle$, a result that holds more generally for any distribution $\rho(\tau)$ whose variance $\langle\tau^2\rangle$ is finite. In the marginal case $\alpha = 2$, one gets $S(t) \sim 1/\ln(t/\tau_o)$. More importantly, when $1 < \alpha < 2$, $S(t) \sim t^{\alpha-2}$, implying that the creep exponent is $p = \alpha - 1$. Though the starting point given by Eq. (6) is different, those conclusions are in agreement with Ref. [30]. We do not consider the case $\alpha < 1$, as we assume that the mean yielding $\langle\tau\rangle$ is finite so that an equilibrated state exists. In the limit $\alpha \to 1^+$, the behavior approaches logarithmic creep, since $\langle\tau\rangle$ grows without bound and there are no more time scale in the system.

While those conclusions have been reached for an exponential $\rho_E(E)$, corresponding to a power law $\rho(\tau)$, they are informative of other situations. First, if yielding times are bounded by a maximal value $\tau_{\max}$, the long-time behavior is ultimately Newtonian but up to $t \simeq \tau_{\max}$, we expect a transient regime similar to the asymptotic behavior described above. Second, as soon as the distribution of energy is not narrowly peaked, there are widely different yielding times, and we expect that the creep exponent directly reflects the width of energy distribution.

With the mean-field prediction in hand, we now examine how the creep properties is affected by the type of stress redistribution and the choice of energy barrier. As a quantitative measure, we focus on the exponent characterizing the primary creep regime. In practice, a linear fit to $\epsilon(t)$ in bilogarithmic scale was used to get at all
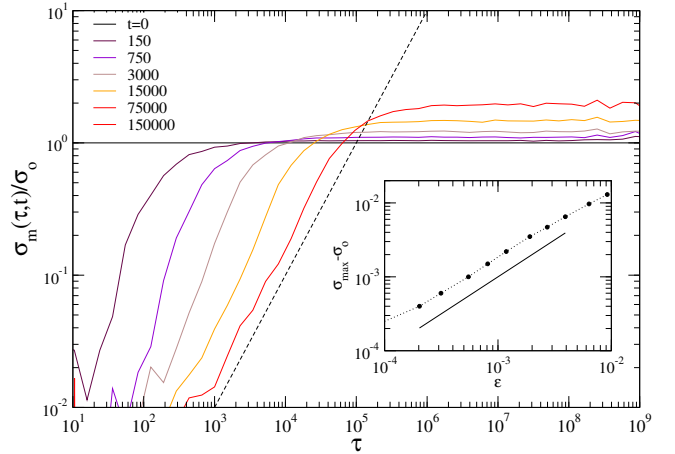

Fig. 3: Analysis of local stress during creep. The main graph shows how the mean stress $\sigma_m(\tau, t)$ carried by sites with yielding time τ evolves in time. A plateau is seen at large τ. (Inset) Plateau value σ_{pl}, indicating the mean stress carried by "slow" elements, as a function of strain. The dashed and solid lines have slope unity. The simulation involves Eshelby redistribution, Gaussian ρ_E with $\Delta = 3$ and $\sigma_o = 0.01$.

time an "effective exponent", the minimum of which is the creep exponent reported in Fig. 2. If ρ_E is exponential, the asymptotic behavior is $\epsilon(t) \sim t^p$, and the minimum is attained in a plateau at the longest time. If ρ_E is Gaussian, or bounded, then $\epsilon(t) = ct^p + t/\eta$ [36], with c a constant and η the viscosity[1]. The effective exponent exhibits a minimum near the crossover between the two regimes, which, to be seen, may require very long simulations, reaching up to 10^9 KMC iterations. As shown in Fig. 2 (top right), the simulation data for the exponential ρ_E is in full agreement with the mean-field prediction $p = \alpha - 1$. Should we expect a similar result with Eshelby and short-range redistributions? On the one hand, given the long-range nature of elastic propagator, the mean-field theory could be expected to be exact [37]. On the other hand, it was argued that the stress resulting from spatially distributed events is "dominated by local contributions" [16,38]. Surprisingly, we find that within numerical accuracy, the mean-field and short-range exponents coincide, whereas the Eshelby case yields consistently higher values. In the Gaussian case, no pronounced difference is seen in the exponents. Overall, we see that the wider the barrier distribution, the slower the creep, but the value of creep exponent is sensitive to both the specific distribution of barriers and the form of the stress propagator.

Local stress. – To get further insight in the mesoscopic dynamics during the creep regime, we have conducted an analysis of the local stress carried by elements. Of particular attention is the relation between the local stress σ_i carried by an element i, and its instantaneous yielding time τ_i. Figure 3 reveals a strongly heteroge-

---

[1]Here the applied stress is so small that fluidization does not occur.

neous dynamics during primary creep. Indeed, "fast" elements having a low energy barrier carry on average a small amount of stress $\sigma_i \ll \sigma_{\rm o}$, while "slow" elements support most of the stress. Noticeably, the level of stress borne by these elements increases with time. As shown in the inset of Fig. 3, this increase is approximately proportional to the local strain $\epsilon(t)$. Such strain hardening, here understood as an increase in local stress required to produce additional strain, may be simply explained in the framework of the mean-field analysis presented above. Using Eqs. (8)-(9), one gets for $\sigma_{\rm m}(\tau, t)$, the mean stress carried at time t by elements with yield time τ,

$$\sigma_{\rm m}(\tau, s) = \frac{\overline{\sigma}(\tau, s)}{P_{\rm st}(\tau)} = \frac{\sigma_{\rm o} + S(s)}{s + \tau^{-1}}. \qquad (10)$$

and obtain in the two limits,

$$\tau \ll t, \qquad \sigma_{\rm m}(\tau, t) = 2\mu\tau\dot{\epsilon}(t), \qquad (11a)$$
$$\tau \gg t, \qquad \sigma_{\rm m}(\tau, t) = 2\mu\epsilon(t) + \sigma_{\rm o}. \qquad (11b)$$

Schematically, one can identify two populations of sites, respectively fast and slow depending on the value of the local yielding time τ as compared to the elapsed time t. On the one hand, the sites that have yielded already and that are carrying a stress decreasing in time as $\dot{\epsilon}(t)$. On the other hand, the resistant sites that have not yielded yet, and who carry a stress increasing as $\epsilon(t)$. In Fig. 3, one sees that Eqs. (11a) and (11b) apply to a good approximation, even though the propagator is of Eshelby type rather than mean-field.

To conclude on the local stress, we note that the strain hardening behavior reported here is distinct from the exhaustion of low energy barriers discussed in the context of elasto-plastic models [39,40]. In the latter, strain hardening originates in the distribution of the local yield stresses shifting with time, as a result of the progressive exhaustion of the weakest sites. In the present case, the distribution of intrinsic barrier is stationary and there is no bias in the renewal of weak sites. Instead, the strain hardening behavior derives from stress accumulation on the strongest sites.

Fluidization time. – At the fluidization transition, the deformation increases sharply, and we have observed strain localization, as already noticed in Ref. [19]. In particular, the standard deviation of the local strain goes through a maximum, which is used to pinpoint the fluidization time $t_{\rm f}$. Figure 4 reveals an exponential dependence of the fluidization time on the applied stress.

To rationalize this behavior, we make use of two observations. First, the strain at fluidization $\epsilon_{\rm f} = \epsilon(t_{\rm f})$ varies only weakly with $\sigma_{\rm o}$, namely $\epsilon_{\rm f}(\sigma_{\rm o}) \approx \tilde{\epsilon}_{\rm f} - \zeta\sigma_{\rm o}$, as previously observed in some experiments [2,10]. Second, the particular form of $h(\sigma)$ does not appear to have the leading role in the $t_{\rm f}(\sigma_{\rm o})$ relation since we also found an exponential dependence when $h(\sigma)$ is linear rather than quadratic. Consider the plateau in σ associated to slow sites, which
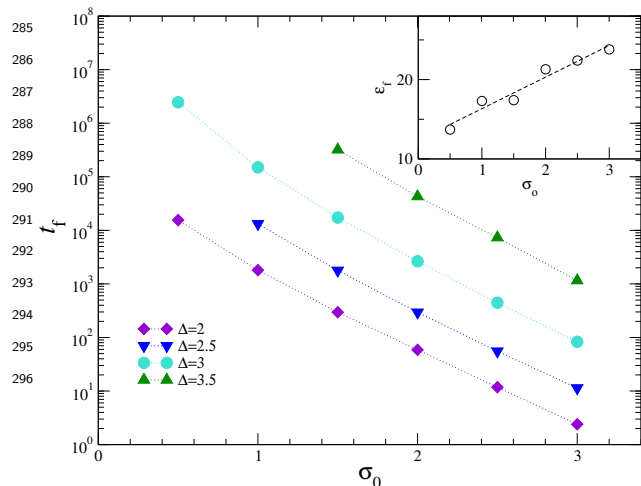

Fig. 4: Fluidization time $t_{\rm f}$ as a function of the applied stress $\sigma_{\rm o}$. Here, redistribution is of Eshelby type, $\rho_{\rm E}$ is Gaussian with width Δ. (Inset) Strain at fluidization $\epsilon_{\rm f}$ as a function of $\sigma_{\rm o}$, for $\Delta = 3$. The dashed line is a linear fit.

at a time t, ranges from t to $\tau_{\rm max}$, the largest relaxation time in the system. We reintroduce the effect of activation in an approximate manner, with $\sigma(t)$ estimated from the solution with no activation term ($h = 0$) found above, thus leading to a shift factor $\exp\left[-h(\sigma_{\rm m}(\tau, t))\right]$ for an element with intrinsic time τ. Now, we postulate that the fluidization occurs where there is no more element whose actual relaxation time is longer than the elapsed time,

$$t_{\rm f} = \tau_{\rm max} \exp\left[-h(\sigma_{\rm o} + 2\mu\epsilon_{\rm f})\right], \qquad (12)$$

that is, activation effects have shifted the longest intrinsic relaxation time to a value equal to $t_{\rm f}$. Assuming $\epsilon_{\rm f}$ is strictly independent of $\sigma_{\rm o}$, and expanding at first order in $\sigma_{\rm o} \ll 2\mu\epsilon_{\rm f}$, one gets

$$t_{\rm f} = C \exp\left[-\sigma_{\rm o}/\tilde{\sigma}\right], \qquad (13)$$

with $C = \tau_{\rm max} \exp\left[-h(2\mu\epsilon_{\rm f})\right]$ and $\tilde{\sigma} = 1/h'(2\mu\epsilon_{\rm f})$. A similar argument applies if $\epsilon_{\rm f}(\sigma_{\rm o})$ exhibits a linear dependence as considered above. As regards the dependence in the width Δ of barrier distribution, we note that the prefactor C may change significantly, as $\tau_{\rm max}$ increases with Δ. In experiments, alongside power law dependence for carbopol gels [41,42], an exponential $t_{\rm f}(\sigma_{\rm o})$ was reported in carbon black gels [8,9], thermo-reversible silica gels [43] and protein gels [44]. Within our mesoscopic model, this phenomenology can be attributed to activated dynamics with energy barriers that are lowered by the applied stress.

Before concluding, we briefly comment on the steady state reached after fluidization, that is characterized by a constant shear rate $\dot{\gamma}$, as observed in colloidal glasses [5]. Simulations show that the final state attained during steady creep is identical to that reached upon constant deformation rate $\dot{\gamma}$. For exponential barrier distribution, the flow curve indicates a power law fluid $\sigma \sim \dot{\gamma}^\alpha$, in agree-

ment with a mean-field analysis. In the Gaussian case, one finds a logarithmic behavior $\sigma \sim \ln(\dot{\gamma})$.

Conclusion. – Through the consideration of a mesoscopic viscoplastic model, we demonstrated that the creep dynamics is directly related to distribution of energy barriers, and to the form of the stress redistribution subsequent to yielding. Moreover, our simulations show that primary creep regime is accompanied by local strain hardening, resulting from the existence of a broad distribution of yielding times. Strain hardening is also key to understand the fluidization process, which here displays an exponential dependence on the applied stress, as seen in experiments on colloidal gels. We believe our model may be relevant for polymeric, metallic or colloidal glasses, in the vicinity of their glass transition temperature or volume fraction. Indeed, the steady state flow in this regime is power law in the case of metallic glasses [3, 45], or logarithmic for polymer glasses [46]. Creep and fluidization are also observed in systems such as carbopol gels [41, 42], which have a yield stress. It remains to address this important class of materials.

REFERENCES

[1] MIGUEL M.-C., VESPIGNANI A., ZAISER M. and ZAPPERI S., *Phys. Rev. Lett.*, **89** (2002) 165501.

[2] BAUER T., OBERDISSE J. and RAMOS L., *Phys. Rev. Lett.*, **97** (2006) 258303.

[3] EGAMI T., IWASHITA T. and DMOWSKI W., *Metals*, **3** (2013) 77.

[4] RIGGLEMAN R. A., SCHWEIZER K. S. and DE PABLO J. J., *Macromolecules*, **41** (2008) 4969.

[5] SIEBENBÜRGER M., BALLAUFF M. and VOIGTMANN T., *Phys. Rev. Lett.*, **108** (2012) 255701.

[6] CHAUDHURI P. and HORBACH J., *Phys. Rev. E*, **88** (2013) 040301(R).

[7] SENTJABRSKAJA T., CHAUDHURI P., HERMES M., POON W. C. K., HORBACH J., EGELHAAF S. U. and LAURATI M., *Sci. Rep.*, **5** (2015) 11884.

[8] GIBAUD T., FRELAT D. and MANNEVILLE S., *Soft Matter*, **6** (2010) 3482.

[9] GRENARD V., DIVOUX T., TABERLET N. and MANNEVILLE S., *Soft Matter*, **10** (2014) 1555.

[10] CATON F. and BARAVIAN C., *Rheol. Acta*, **47** (2008) 601.

[11] BONN D., PAREDES J., DENN M. M., BERTHIER L., DIVOUX T. and MANNEVILLE S., *arXiv*, (2015) 1502.05281.

[12] VOIGTMANN T., *Curr. Opin. Colloid Interface Sci.*, **19** (2014) 549.

[13] LOUCHET F. and DUVAL P., *Int. J. Mater. Res.*, **100** (2009) 1433.

[14] RODNEY D., TANGUY A. and VANDEMBROUCQ D., *Modelling Simul. Mater. Sci. Eng.*, **19** (2011) 083001.

[15] BULATOV V. V. and ARGON A. S., *Modelling Simul. Mater. Sci. Eng.*, **2** (1999) 167.

[16] PICARD G., AJDARI A., LEQUEUX F. and BOCQUET L., *Eur. Phys. J. E.*, **15** (2004) 371.

[17] MARTENS K., BOCQUET L. and BARRAT J.-L., *Phys. Rev. Lett.*, **106** (2011) 156001.

[18] NICOLAS A., MARTENS K., BOCQUET L. and BARRAT J.-L., *Soft Matter*, **10** (2014) 4648.

[19] FIELDING S., *Rep. Prog. Phys.*, **77** (2014) 102601.

[20] BOUTTES D. and VANDEMBROUCQ D., *AIP Conference Proceedings*, (2013) 481.

[21] HOMER E. R., RODNEY D. and SCHUH C. A., *Phys. Rev. B*, **81** (2010) 064204.

[22] ESHELBY J., *Proc. R. Soc. London, Ser. A*, **241** (1957) 467.

[23] DAEHN G. S., *Acta Mater.*, **49** (2001) 2017.

[24] MARTENS K., BOCQUET L. and BARRAT J.-L., *Soft Matter*, **8** (2012) 4197.

[25] HASAN O. A. and BOYCE M. C., *Polym. Eng. Sci.*, **35** (1995) 331344.

[26] SHIRMACHER W., RUOCCO G. and MAZZONE V., *Phys. Rev. Lett.*, **115** (2015) 015901.

[27] XIA X. and WOLYNES P. G., *Phys. Rev. Lett.*, **86** (2001) 5526.

[28] MONTHUS C. and BOUCHAUD J.-P., *J. Phys. A: Math. Gen.*, **29** (1996) 3847.

[29] BORTZ A. B., KALOS M. H. and LEBOWITZ J. L., *J. Comput. Phys.*, **17** (1975) 10.

[30] FIELDING S. M., SOLLICH P. and CATES M. E., *J. Rheol*, **44** (2000) 323.

[31] SOLLICH P., *Phys. Rev. E*, **58** (1998) 738.

[32] HIDALGO R., KUN F. and HERRMANN H., *Phys. Rev. E*, **65** (2002) 032502.

[33] PRADHAN S., HANSEN A. and CHAKRABARTI B. K., *Rev. Mod. Phys.*, **82** (2010) 499.

[34] FINDLEY W., LAI J. and ONARAN K., *Creep and relaxation of nonlinear viscoelastic materials* (Dover) 1978.

[35] FELLER W., *An introduction to probability theory and its applications, Volume II* 2nd Edition (John Wiley & Sons) 1971.

[36] GUEGUEN Y., KERYVIN V., ROUXEL T., LE-FUR M., ORAIN H., BUREAU B., BOUSSARD-PLÉDEL C. and SANGLEBOEUF J.-C., *Mechanics of Materials*, **85** (2015) 47.

[37] DAHMEN K., BEN-ZION Y. and UHL J., *Phys. Rev. Lett.*, **102** (2009) 175501.

[38] FIELDING S. M., CATES M. E. and SOLLICH P., *Soft Matter*, **5** (2009) 2378.

[39] TALAMALI M., PETÄJÄ V., VANDEMBROUCQ D. and ROUX S., *C. R. Mecanique*, **340** (2012) 275.

[40] TYUKODI B., LEMARCHAND C. A., HANSEN J. S. and VANDEMBROUCQ D., *Phys. Rev. E*, **93** (2016) 023004.

[41] DIVOUX T., TAMARII D., BARENTIN C. and MANNEVILLE S., *Phys. Rev. Lett.*, **104** (2010) 208301.

[42] DIVOUX T., TAMARII D., BARENTIN C., TEITEL S. and MANNEVILLE S., *Soft Matter*, **8** (2012) 4151.

[43] GOPALAKRISHNAN V. and ZUKOSKI C. F., *J. Rheol.*, **51** (2007) 623.

[44] LINDSTRÖM S. B., KODGER T. E., SPRAKEL J. and WEITZ D. A., *Soft Matter*, **8** (2012) 3657.

[45] SPAEPEN F., *Acta Metall.*, **25** (1977) 407.

[46] WARD I. M. and SWEENEY J., *An introduction to the mechanical properties of solid polymers* (Wiley) 2004.